

A mechanism for preseismic steady rupture fronts observed in laboratory experiments

Y. Kaneko¹ and J.-P. Ampuero²

Received 10 October 2011; accepted 11 October 2011; published 10 November 2011.

[1] It has been shown that the onset of frictional instability is characterized by a transition from stable, quasi-static rupture growth to unstable, inertially-controlled high-speed rupture. In particular, slow rupture fronts propagating at a steady speed V_{slow} of the order of 5% of the S -wave speed have been observed prior to the onset of dynamic rupture in recent fault-friction laboratory experiments. However, the precise mechanism governing this V_{slow} stage is unknown. Here we reproduce this phenomenon in numerical simulations of earthquake sequences that incorporate laboratory-derived rate-and-state friction laws. Our simulations show that the V_{slow} stage originates from a stress concentration inherited from the coalescence of interseismic slow creep fronts. Its occurrence is limited to a narrow range of the parameter space but is found in simulations with two commonly-used state-variable evolution laws in the rate-and-state formulation. The sensitivity of the speed V_{slow} to the model parameters suggests that the propagation speed V_{slow} reported in laboratory experiments may also be sensitive to parameters of friction and stress conditions. Our results imply that time and space dimensions associated with the propagation of V_{slow} on natural faults can be as much as a few seconds and several hundred meters, respectively. Hence the detection of such preseismic signals may be possible with near-field high-resolution observations. **Citation:** Kaneko, Y., and J.-P. Ampuero (2011), A mechanism for preseismic steady rupture fronts observed in laboratory experiments, *Geophys. Res. Lett.*, 38, L21307, doi:10.1029/2011GL049953.

1. Introduction

[2] The onset of frictional instability is a key mechanism governing the nucleation of crustal earthquakes and landslides. It has been demonstrated both in laboratory experiments [e.g., Dieterich, 1979; Ruina, 1983; Dieterich and Kilgore, 1996; Ohnaka and Shen, 1999; Nielsen et al., 2010] and numerical simulations [e.g., Okubo, 1989; Rice and Ben-Zion, 1996; Lapusta et al., 2000; Rubin and Ampuero, 2005] that the onset of frictional instability is characterized by a transition from stable, quasi-static rupture growth to unstable, inertially-controlled high-speed rupture. While these studies have advanced our understanding of the transitional behavior, direct comparisons between numerical

models and laboratory observations remain quite challenging due to difficulties in accurately monitoring the transitional behavior in laboratory friction experiments and in reproducing the laboratory observations in numerical simulations that incorporate appropriate friction laws.

[3] Several laboratory studies attempted to understand the behavior of the quasi-static to dynamic transition of stick-slip motion on experimental faults (i.e., pre-cut interfaces). Ohnaka and Shen [1999] reported an initial, quasi-static phase in which the rupture grows at a slow and steady speed, followed by a rupture acceleration phase up to dynamic speeds. In friction experiments on polymethyl-methacrylate (PMMA), Rubinstein et al. [2004] observed a slow detachment front propagating at 5% of the S -wave speed (V_s) after the passage of a supershear rupture front. More recently, Nielsen et al. [2010] reported steady rupture fronts systematically propagating at about 5% of V_s on experimental faults where a stick-slip instability was spontaneously nucleated under slow loading. However, under different loading conditions, Ben-David et al. [2010] found variability of rupture speeds ranging from a few percent of V_s to P -wave speed (V_p) depending on the ratio of local shear to normal stresses, suggesting that the speed of slow steady fronts (~5% of V_s) observed in Rubinstein et al. [2004] and Nielsen et al. [2010] is not universal. Hence the mechanism of a slow steady propagation front remains elusive.

[4] In this study, we reproduce the occurrence of slow steady propagation fronts preceding fast dynamic rupture in numerical simulations of spontaneous earthquake sequences, consistent with the laboratory findings of Nielsen et al. [2010]. We refer to this phenomenon as a ' V_{slow} stage' and to its propagation speed as ' V_{slow} '. We discuss the mechanism of the V_{slow} stage, the dependence of V_{slow} on model parameters, and its potential occurrence on natural faults.

2. Model Set-Up

[5] We conduct 2-D simulations of spontaneous earthquake sequences on a 1-D fault subjected to slow, tectonic loading [Kaneko et al., 2010]. We consider an antiplane (Mode III) configuration in which purely dip-slip motion is assumed. The simulations resolve all stages of the seismic cycle: the aseismic nucleation process, the subsequent dynamic rupture event, the postseismic slip, and the interseismic quasi-static deformation.

[6] The fault resistance to sliding is described by laboratory-derived rate and state friction laws [Dieterich, 1979; Rice and Ruina, 1983; Ruina, 1983]. For time-independent effective normal stress $\bar{\sigma}$, the shear strength τ on the fault is expressed as

$$\tau = \bar{\sigma} [f_0 + a \ln(\delta/\delta_0) + b \ln(\delta_0\theta/L)], \quad (1)$$

¹Institute of Geophysics and Planetary Physics, Scripps Institution of Oceanography, University of California, San Diego, La Jolla, California, USA.

²Division of Geological and Planetary Sciences, California Institute of Technology, Pasadena, California, USA.

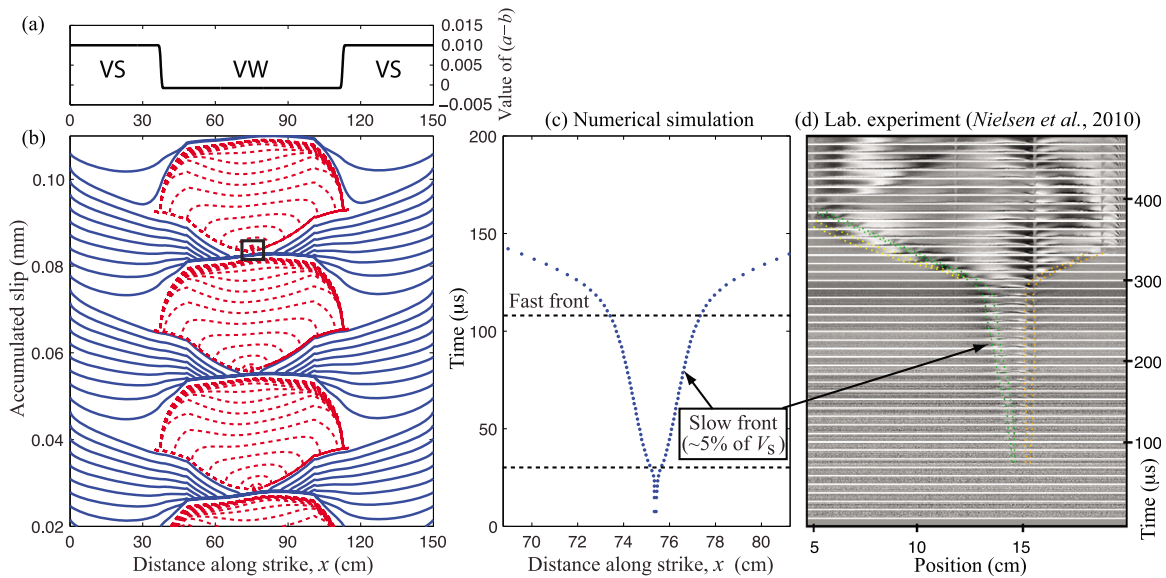


Figure 1. An example of preseismic slow-propagation fronts ($\sim 5\%$ of V_s) in long-term fault-slip simulations. (a) The assigned distribution of the friction parameter ($a - b$) with $a = 0.0100$, $b = 0.0108$, and $a/b = 0.93$ in the velocity-weakening (VW) segment and $a = 0.0100$ and $b = 0$ in the velocity-strengthening (VS) segments. (b) The assigned distribution of the friction parameter results in a sequence of shear-slip events similar to that in the laboratory experiments of *Nielsen et al.* [2010]. Red and blue curves display slip accumulation every $25 \mu\text{s}$ during the simulated earthquakes and every 0.55 hours, respectively. The black square indicates a location where one of the seismic events nucleates. (c) Positions of the rupture fronts as a function of time during a transition from quasi-static to dynamic rupture. Time $t = 0$ is chosen sometime before the V_{slow} stage. The rupture fronts, defined as the locations of peak shear stresses, propagate bilaterally with two distinct speeds: $V_r \sim 0.05V_s$ (slow front) and $V_r \gg 0.05V_s$ (fast front). (d) A sequence of interferometric photograms showing the nucleation and the propagation of rupture fronts in laboratory experiments (image based on Figure 1 of *Nielsen et al.* [2010]).

where a and b are rate and state constitutive parameters, $\dot{\delta}$ is slip velocity, f_0 is a reference friction coefficient corresponding to a reference slip velocity $\dot{\delta}_0$, θ is a state variable, and L is the characteristic slip for state evolution [e.g., *Dieterich, 1979; Ruina, 1983; Rice and Ruina, 1983*]. We consider the two most classical state variable evolution laws:

$$d\theta/dt = 1 - \dot{\delta}\theta/L \quad (\text{aging law}), \quad (2)$$

$$d\theta/dt = -(\dot{\delta}\theta/L) \ln(\dot{\delta}\theta/L) \quad (\text{slip law}) \quad (3)$$

[*Dieterich, 1979; Ruina, 1983*]. Recently, *Ampuero and Rubin* [2008] rekindled the discussion of which state evolution laws are more appropriate to use in earthquake modeling. *Bayart et al.* [2006] showed that the slip law provides a better match to velocity-jump experiments. On the other hand, *Beeler et al.* [1994] found, during slide-hold-slide experiments using a servo-control system, that a frictional surface heals with time, rather than with slip rate, suggesting that the aging law is a more appropriate representation.

[7] The parameter combination $a - b < 0$ corresponds to steady-state velocity-weakening friction and can lead to unstable slip, whereas $a - b > 0$ corresponds to steady-state velocity-strengthening and leads to stable sliding. Throughout this article, we omit the words “steady-state” and simply refer to velocity weakening or strengthening.

[8] Under slow tectonic loading, a frictional instability (i.e., an earthquake) is able to develop only if the velocity-

weakening region of the fault exceeds the nucleation size h^* [*Rice and Ruina, 1983; Rubin and Ampuero, 2005*]. Two theoretical estimates of the earthquake nucleation size for 2-D problems are given by

$$h_{\text{RR}}^* = \frac{\pi}{4} \frac{\mu L}{\bar{\sigma}(b-a)}, \quad (4)$$

$$h_{\text{RA}}^* = \frac{2}{\pi} \frac{\mu L b}{\bar{\sigma}(b-a)^2}, \quad (5)$$

where μ is shear modulus for mode III. The estimate h_{RR}^* was derived from the linear stability analysis of steady sliding by *Rice and Ruina* [1983], while h_{RA}^* was obtained for $a/b \gtrsim 0.5$ by *Rubin and Ampuero* [2005] on the basis of energy balance for a quasi-statically expanding crack governed by the aging law (2). *Rubin and Ampuero* [2005] gave formulae for half of the nucleation size but we use full sizes.

[9] Our simulated fault is 300-cm long. Slip evolution is computed based on the assumed friction law on the 150-cm long central portion. The slip rate $\dot{\delta}_{\text{Load}} = 5$ cm/year is prescribed on the two 75-cm long outer portions of the fault. The central portion is divided into three segments: a 75-cm long velocity-weakening segment surrounded by two 37.5-cm long velocity-strengthening segments (Figure 1a). The velocity-strengthening segments mimic viscous silicon patches placed at each end of the fault in some of the experiments of *Nielsen et al.* [2010], creating similar loading

Table 1. A Range of Parameters Used in This Study

Parameter	Symbol	Slip-Law Cases	Aging-Law Cases
Shear modulus	μ	32.0 GPa	32.0 GPa
Shear wave speed	V_s	3.464 km/s	3.464 km/s
Reference slip rate	$\dot{\delta}_0$	10^{-6} m/s	10^{-6} m/s
Reference friction coefficient	f_0	0.6	0.6
Characteristic slip	L	0.1 microns	0.1 microns
Effective normal stress	$\bar{\sigma}$	50 MPa	50 MPa
Rate-and-state parameter a	a	0.0100	0.0100
Rate-and-state parameter b	b	0.0105 – 0.0140 ^a	0.0108 – 0.0140 ^a
Size of velocity-weakening segment	D_{vw}	50–112 cm	56–100 cm
Loading rate	$\dot{\delta}_{Load}$	1–100 cm/yr	5 cm/yr

^aThe indicated values of b are valid for the VW region.

conditions. Note that, in the study of *Nielsen et al.* [2010], the V_{slow} stage was observed for smooth fault surfaces with or without viscous patches (S. Nielsen, written communication, 2009), but was not observed for rough surfaces with viscous patches.

[10] Table 1 gives a range of model parameters considered in this study. Since values of rate-and-state parameters a , b , and L are not known for the laboratory specimen of *Nielsen et al.* [2010], we do not attempt to exactly reproduce the spatial and temporal scales of the V_{slow} stage observed in their laboratory experiments. Instead, we set the spatial scale and nucleation sizes to be roughly equal to those in the laboratory experiments by adjusting the value of L . The values of other model parameters are chosen to represent plausible stress and friction values on natural faults in seismogenic conditions rather than those in the laboratory experiments.

3. Simulations of Slow Steady Propagation Fronts

[11] Figure 1 shows one of the simulation examples in which slow steady fronts (V_{slow}) propagate at about 5% of V_s systematically during the nucleation processes of seismic events. Motivated by the fact that a/b of many velocity-weakening materials in laboratory experiments is closer to 1 than 0, we set $a/b = 0.93$. In this example (Figure 1b) we adopt the slip law (3). The blue lines show the continuous slow sliding of the velocity-strengthening segments, which creates a stress concentration at its tip and penetrates into the velocity-weakening segment (Figure 1b). In due time, seismic rupture nucleates and propagates bilaterally (its progression is shown by red lines in Figure 1b). After a seismic event, the velocity-strengthening segments experience postseismic sliding due to the transferred stress. The interseismic period between two successive events is 5 hours.

[12] Figure 1c shows a close-up look at the onset of one of the seismic events. The rupture fronts, the positions of which are defined here by the peak values of shear stress, begin at a localized point, expand quasi-statically, then steadily propagate at about 5% of V_s before accelerating to much faster speeds. The behavior of the V_{slow} fronts (Figure 1c) is similar to that in the laboratory experiments of *Nielsen et al.* [2010] (Figure 1d) in that the speed V_{slow} is about 5% of V_s and remains about the same for all events in a given simulation (except for the first few that are affected by initial conditions).

[13] To understand the mechanism of the slow steady fronts, we look at the evolution of slip rates $\dot{\delta}$, shear stress, and the quantity $\dot{\delta}\theta/L$ before and during the occurrence of

the V_{slow} stage (Figure 2). During the interseismic period, two creep fronts emanate from the rheological boundaries ($x \approx 45, 105$ cm) and then propagate inward. Their eventual coalescence creates favorable conditions for earthquake nucleation near the center of the fault (Figures 2a, 2c, and 2e). Behind the two creep fronts, the condition is near steady-state ($\dot{\delta}\theta/L \approx 1$), and there is no evolution of state variable θ according to (3). The V_{slow} stage originates from a stress concentration inherited from the coalescence of the creep fronts (Figures 2b, 2d, and 2f). During the V_{slow} stage, the peak slip velocities remain roughly constant in time (~ 0.05 m/s in this example). The expansion of rupture takes the form of a bilateral crack (Figure 2b) as opposed to a unilateral pulse reported by *Ampuero and Rubin* [2008] under different loading conditions.

[14] The relation between propagation speed V_{slow} and peak slip rate $\dot{\delta}_{max}$ is consistent with a theoretical relation given by equation (53) of *Ampuero and Rubin* [2008]:

$$V_{prop} \approx 0.75 \frac{\mu \dot{\delta}_{max}}{b\bar{\sigma}} \left(\ln \frac{\dot{\delta}_{max} \theta_i}{L} \right)^{-1}, \quad (6)$$

where θ_i is the value of the state variable prior to the arrival of the rupture front. For instance, for the case shown in Figure 2, $\ln(\dot{\delta}_{max} \theta_i/L) \approx 11-16$ and $\dot{\delta}_{max} \sim 0.05$ m/s, which yields $V_{prop}/V_s = 0.04-0.06$. This is consistent with the speed V_{slow} obtained in the simulation (Figure 1c).

[15] Setting $\dot{\delta}_{max} = 2a\sigma V_s/\mu$ in (6), the slip velocity at which the effect of radiation damping is comparable to the direct effect of rate-and-state friction, *Perfettini and Ampuero* [2008] proposed that a typical rupture speed at the onset of elastodynamic effects was $V_{prop} \sim 0.05V_s$. To assess the relevance of elastodynamics, Figure 2 shows results obtained by first simulating three earthquake cycles (Figure 1b), then continuing with a quasi-static simulation (by turning off the inertial effects). We find that the V_{slow} stage occurs despite the quasi-static assumption, suggesting that the speed V_{slow} does not explicitly depend on V_s . A subtle effect of elastodynamics is however not discarded because the arrest of the last dynamic event sets the background conditions for the creep front propagation.

[16] A fracture mechanics argument based on an idealized model provides insight on how the stress concentration induced by the coalescence of the creep fronts gives rise to a period of a steady propagation speed. Let us consider the quasi-static growth of a mode III crack of length 2ℓ under a stress field that consists of a uniform background value (and hence constant stress drop $\Delta\tau$) plus a highly concentrated

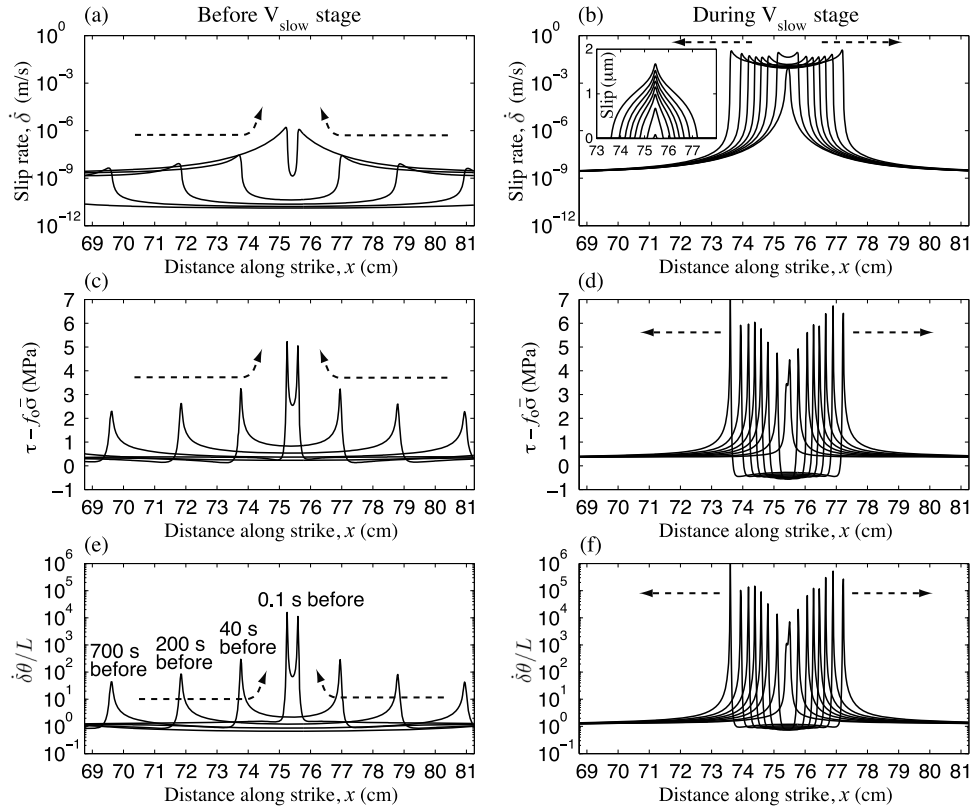


Figure 2. Snapshots of (a, b) slip rates, (c, d) shear stress τ with respect to a reference stress value $f_0\bar{\sigma}$, and (e, f) $\delta\theta/L$, before and during the V_{slow} stage. Each snapshot in Figures 2a, 2c, and 2e is taken at times before the onset of the V_{slow} stage indicated in Figure 2e. Snapshots in Figures 2b, 2d, and 2f are taken every $13 \mu\text{s}$. Arrows indicate the propagation direction of the peak values in each plot. The inset in Figure 2b shows slip accumulation during the V_{slow} stage, indicating a crack-like expansion of rupture growth. The propagation of V_{slow} originates from a stress concentration inherited from the coalescence of the slow creep fronts. The result from a quasi-static simulation is shown, and the outermost curves in Figures 2b, 2d, and 2f correspond to the time just before the quasi-static solution ceased to exist.

force F at the center of the crack. The balance between the energy release rate at the crack tip, G , and the fracture energy, G_c , provides a relation between crack speed V_{prop} and crack half-length ℓ . On the one hand, the static energy release rate G , given by [e.g., *Ampuero et al.*, 2006]

$$G(\ell) = \frac{\pi\ell}{2\mu} \left(\overline{\Delta\tau} + \frac{2F}{\pi\ell} \right)^2, \quad (7)$$

reaches a minimum when $\ell = \ell_{\text{min}} = 2F/(\pi\overline{\Delta\tau})$. On the other hand, the effective fracture energy of rate-and-state friction behaves as $G_c \approx b\bar{\sigma}\text{Ln}(\delta_{\text{max}}/\delta_{\text{Load}})^n$, where $n = 1$ for the slip law and $n = 2$ for the aging law [*Ampuero and Rubin*, 2008]. Equation (6) implies that δ_{max} , and hence G_c , is an increasing function of V_{prop} . Since $G(\ell) = G_c(V_{\text{prop}})$, the crack propagation speed is almost steady when the energy release rate $G(\ell)$ is almost constant. This happens when the crack length is close to $2\ell_{\text{min}}$. This analysis shows that a quasi-statically expanding crack subjected to a stress concentration can lead to a period of a steady propagation speed. The previous analysis also provides an estimate of the propagation speed, which depends on the product $F\overline{\Delta\tau}$. However, deriving an adequate estimate of F is not straightforward, and the quantitative comparison of the

idealized model to the numerical simulation results remains a subject of future work.

4. Dependence of the Speed of Steady Propagation Fronts on Model Parameters

[17] To identify the parameters controlling V_{slow} , we perform a number of earthquake-sequence simulations with different sets of model parameters indicated in Table 1. First, we vary the size of the velocity-weakening segment D_{vw} while other parameters are held fixed. We normalize D_{vw} by $h^*_{\text{RR}}/2$, a length that agrees well with our simulated nucleation sizes. We find that by increasing D_{vw}/h^* the speed V_{slow} increases (Figure 3a), the duration of the V_{slow} stage decreases dramatically, and its spatial extent remains about the same (Figure 3b).

[18] Different speeds of V_{slow} fronts (Figure 3a) are related to different amplitudes of slow creep fronts during the interseismic period. For a larger value of D_{vw}/h^* , the slip rate of slow creep fronts is larger (e.g., $\sim 10^{-8}$ vs. $\sim 10^{-9}$ m/s in Figure 3c) and, upon their coalescence, the resulting peak slip rate (δ_{max}) during the V_{slow} stage also becomes larger (Figure 3c). From (6), the speed V_{slow} is strongly correlated to the peak slip rate (Figure 3b). Hence the coalescence of

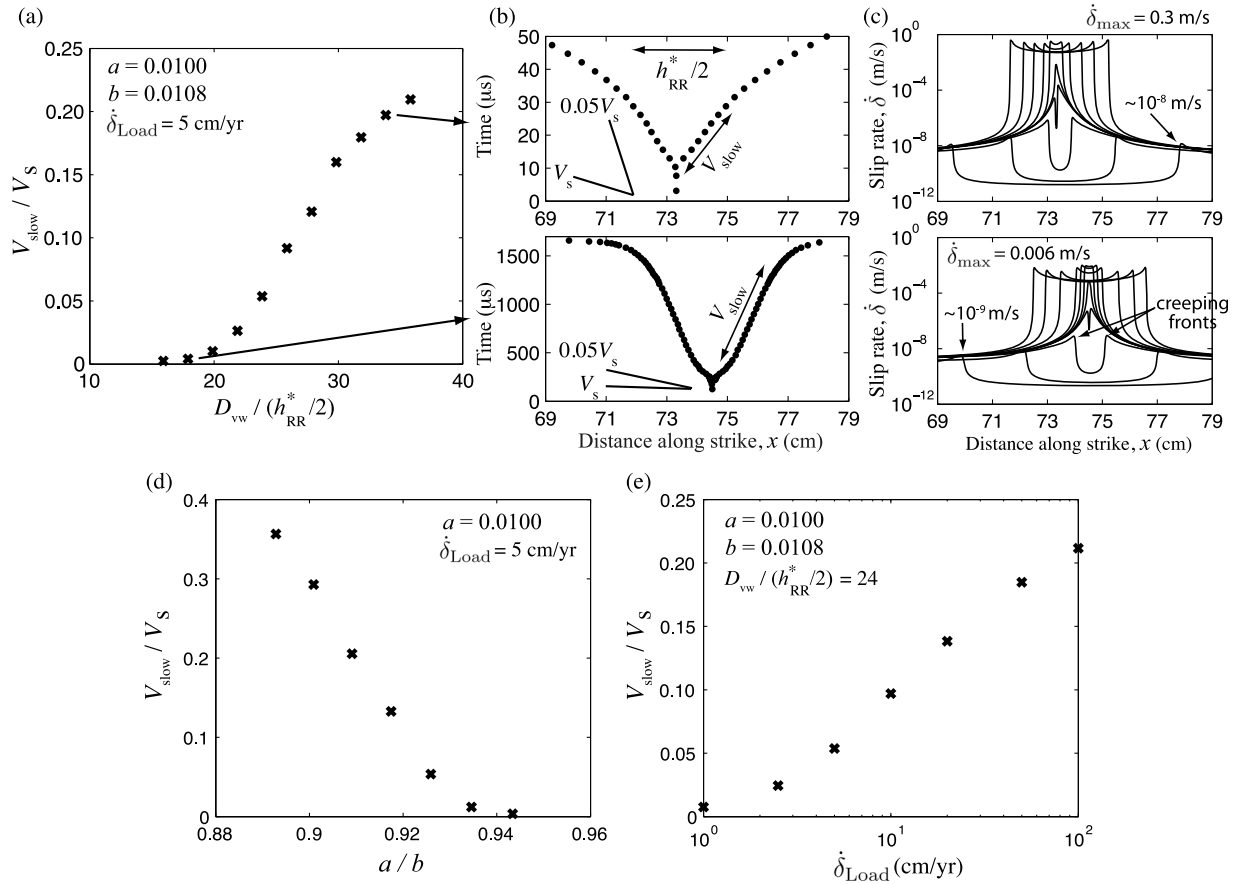


Figure 3. Dependence of the speed V_{slow} of slow propagation fronts on model parameters. (a) V_{slow}/V_s vs. the size of the velocity-weakening segment D_{vw} divided by a theoretical estimate of the nucleation size $h_{\text{RR}}^*/2$, with $h_{\text{RR}}^*/2 = 3.1 \text{ cm}$ for the parameters used. V_{slow} increases with D_{vw}/h^* . The evolution of (b) peak shear stress and (c) slip rates for two end-member cases shown in Figure 3a. Top plots in Figures 3b and 3c correspond to the same case. The peak slip rates during the V_{slow} stage and of the slow creeping fronts during the interseismic period are an order of magnitude larger for the case with larger V_{slow} . (d) V_{slow}/V_s vs. a/b in the velocity-weakening segment, with $a = 0.01$. V_{slow} decreases as a/b increases. (e) V_{slow}/V_s vs. the loading rate $\dot{\delta}_{\text{Load}}$. Note that the horizontal axis is on a logarithmic scale. V_{slow} increases with the loading rate. Indicated parameters and their values are held unchanged for the results shown in Figures 3a, 3d, and 3e.

larger-amplitude creep fronts emerging during the interseismic period leads eventually to a faster propagation speed during the V_{slow} stage.

[19] We also vary the value of the rate-and-state parameter b in the velocity-weakening segment. We find that V_{slow} decreases with increasing a/b (Figure 3d). This behavior can be attributed to the dependence of V_{slow} on D_{vw}/h^* shown in Figure 3a, which indicates that a smaller nucleation size h^* leads to a faster V_{slow} ; theoretical estimates (4) and (5) and numerical simulations show that h^* generally decreases as b increases. When a/b becomes even smaller ($a/b < 0.88$), the nucleation occurs near one of the rheological transitions and takes the form of a unilateral pulse (Figures 4a and 4d). Since the nucleation size becomes smaller and the fault becomes more unstable with larger $b - a$, one of the slow creep fronts can self-accelerate towards earthquake nucleation, without coalescence (Figure 4d). Its peak slip rate increases monotonically with time, and so does its propagation speed as predicted by (6) (Figures 4a and 4d). Hence there is no steady V_{slow} stage when the nucleation occurs near one of the rheological transitions (Figures 4a and 4d).

This behavior was also observed by Nielsen *et al.* [2010] in experiments with rough surfaces and viscous patches. We find that this style of nucleation is the most common in the parameter range shown in Table 1. This is probably why a V_{slow} stage was not reported in previous theoretical studies.

[20] Since the assumed loading rate $\dot{\delta}_{\text{Load}}$ is orders of magnitudes slower than that in the laboratory experiments, we further explore the dependence of V_{slow} on $\dot{\delta}_{\text{Load}}$. Figure 3e shows that the speed V_{slow} increases with the loading rate. Kaneko and Lapusta [2008] demonstrated how increased loading conditions could change the nucleation process and, in particular, cause order-of-magnitude smaller nucleation sizes. Since a larger loading rate leads to a smaller nucleation size, the quantity D_{vw}/h^* increases with the loading rate, resulting in larger V_{slow} in our simulations (Figure 3e).

[21] We also find the occurrence of a V_{slow} stage in simulations with the aging law (2) (Figure 4c). The dependence of the properties of the V_{slow} stage on model parameters is qualitatively similar to the case of the slip law, although the parameter ranges in which a V_{slow} stage occurs

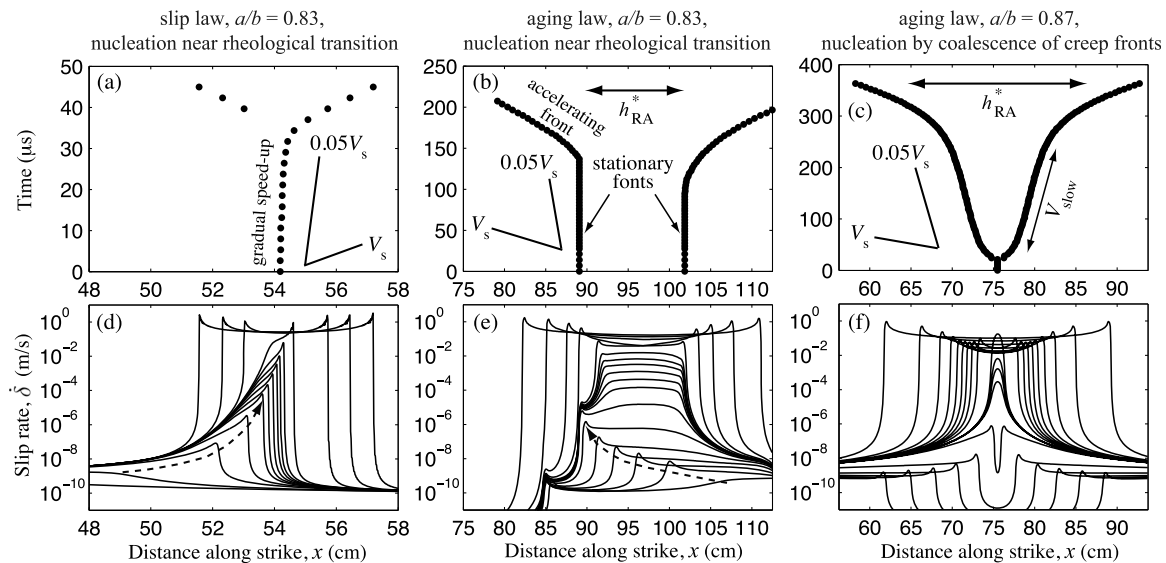


Figure 4. Nucleation processes for the cases with (a, d) the slip law and $a/b = 0.83$, (b, e) the aging law and $a/b = 0.83$, and (c, f) the aging law and $a/b = 0.87$. The evolution of peak shear stress (Figures 4a–4c) and slip rates (Figures 4d–4f) in each case is shown. A theoretical estimate of the nucleation size h_{RA}^* given in (5) is indicated for the cases with the aging law. In Figures 4d and 4e, the nucleation occurs near the rheological transition where a slow creep front becomes unstable. Arrows in Figures 4d and 4e indicate the propagation direction of the slow creep front. In Figure 4f, the coalescence of two slow creep fronts during the interseismic period leads to a nucleation characterized by the V_{slow} stage prior to the onset of the unstable rupture.

are different. Under the same rate and state parameters, $V_{slow} \sim 0.05V_s$ when $D_{vw}/h^* \sim 24$ for the slip law and $D_{vw}/h^* \sim 3.4$ for the aging law, respectively (Figures 4a and 4b). For both laws a V_{slow} stage exists when nucleation proceeds by coalescence of two slow creeping fronts (Figures 4c and 4f), but not if nucleation occurs near a rheological transition (Figures 4b and 4e).

5. Discussion

[22] We have found that in rupture models nucleated by the coalescence of aseismic slip fronts, dynamic rupture is preceded by a stage of slow, steady rupture propagation. Its rupture speed V_{slow} is not universal, but depends on frictional and loading parameters (Figures 3 and 4). This suggests that the value $V_{slow} \sim 0.05V_s$ reported in the laboratory experiments of Nielsen *et al.* [2010] may also be sensitive to parameters of friction and stress conditions. Future work may be directed towards determining the values of the rate- and state parameters of the laboratory specimen to allow quantitative comparison between laboratory observations and numerical simulations.

[23] Slow propagation fronts have been observed in laboratory experiments under a variety of loading conditions [e.g., Rubinstein *et al.*, 2004; Nielsen *et al.*, 2010; Ben-David *et al.*, 2010]. In this study, the occurrence of a V_{slow} stage results from coalescence of slow creep fronts emanating from rheological boundaries, and hence loading conditions play an important role in generating a V_{slow} stage. We have not yet explored scenarios where the fault is characterized by velocity-weakening conditions only (i.e., no rheological transitions). Whether the V_{slow} stage would occur under such scenarios remains a subject of future work.

[24] Earthquake nucleation is relevant to earthquake prediction because nucleation determines the origin time and hypocenter of seismic rupture and may result in detectable precursors. Laboratory rock-sliding experiments showed that values of characteristic slip L range from ~ 1 to $\sim 500 \mu\text{m}$, depending on the fault roughness and gouge width [Marone, 1998]. Space dimension in numerical models can be non-dimensionalized, for example, by $x^* = x/L$ such that the results of numerical simulations can be scaled with L . The results shown in Figures 1c and 4c combined with the upper bound of the laboratory value $L = 500 \mu\text{m}$ suggest that the space and time dimensions associated with hypothetical V_{slow} fronts propagating at 5% of V_s on natural faults correspond to ~ 100 m and ~ 0.6 s ($= 100$ m divided by $0.05V_s$) for the cases with the slip law, respectively, and ~ 500 m and ~ 3 s ($= 500$ m divided by $0.05V_s$) for the cases with the aging law, respectively. This implies that inferences of such preseismic steady rupture propagation before the break-out of a seismic event may be possible with near-field high-resolution observations.

[25] **Acknowledgments.** The authors thank Stefan Nielsen for sharing the results of his laboratory experiments. The reviews by Maria Elina Belardinelli and an anonymous reviewer helped us improve the manuscript. This study was supported by NSF (grant EAR-1015698) and SCEC (funded by NSF Cooperative Agreement EAR-0106924 and USGS Cooperative Agreement 02HQAG0008). This is SCEC contribution number 1511.

[26] The Editor thanks Maria Elina Belardinelli and an anonymous reviewer for their assistance in evaluating this paper.

References

Ampuero, J.-P., and A. M. Rubin (2008), Earthquake nucleation on rate and state faults: Aging and slip laws, *J. Geophys. Res.*, *113*, B01302, doi:10.1029/2007JB005082.

- Ampuero, J.-P., J. Ripperger, and P. M. Mai (2006), Properties of dynamic earthquake ruptures with heterogeneous stress drop, *Earthquakes: Radiated Energy and the Physics of Faulting*, *Geophys. Monogr. Ser.*, vol. 170, 255–261, edited by R. Abercrombie et al., AGU, Washington, D. C.
- Bayart, E., A. M. Rubin, and C. Marone (2006), Evolution of fault friction following large velocity jumps, *Eos Trans. AGU*, 87(52), Fall Meet. Suppl., Abstract S31A-0180.
- Beeler, N. M., T. E. Tullis, and J. D. Weeks (1994), The roles of time and displacement in the evolution effect in rock friction, *Geophys. Res. Lett.*, 21, 1987–1990, doi:10.1029/94GL01599.
- Ben-David, O., G. Cohen, and J. Fineberg (2010), The dynamics of the onset of frictional slip, *Science*, 330, 211–214, doi:10.1126/science.1194777.
- Dieterich, J. H. (1979), Modeling of rock friction: 1. Experimental results and constitutive equations, *J. Geophys. Res.*, 84, 2161–2168, doi:10.1029/JB084iB05p02161.
- Dieterich, J. H., and B. H. Kilgore (1996), Implications of fault constitutive properties for earthquake prediction, *Proc. Natl. Acad. Sci. U. S. A.*, 93(9), 3787–3794.
- Kaneko, Y., and N. Lapusta (2008), Variability of earthquake nucleation in continuum models of rate-and-state faults and implications for after-shock rates, *J. Geophys. Res.*, 113, B12312, doi:10.1029/2007JB005154.
- Kaneko, Y., J.-P. Avouac, and N. Lapusta (2010), Towards inferring earthquake patterns from geodetic observations of interseismic coupling, *Nat. Geosci.*, 3, 363–369, doi:10.1038/NGEO843.
- Lapusta, N., J. Rice, Y. Ben-Zion, and G. Zheng (2000), Elastodynamic analysis for slow tectonic loading with spontaneous rupture episodes on faults with rate- and state-dependent friction, *J. Geophys. Res.*, 105(B10), 23,765–23,789, doi:10.1029/2000JB900250.
- Marone, C. (1998), Laboratory-derived friction laws and their application to seismic faulting, *Annu. Rev. Earth Planet. Sci.*, 26, 643–696, doi:10.1146/annurev.earth.26.1.643.
- Nielsen, S., J. Taddeucci, and S. Vinciguerra (2010), Experimental observation of stick-slip instability fronts, *Geophys. J. Int.*, 180, 697–702, doi:10.1111/j.1365-246X.2009.0444.x.
- Ohnaka, M., and L. F. Shen (1999), Scaling of the shear rupture process from nucleation to dynamic propagation: Implications of geometric irregularity of the rupturing surfaces, *J. Geophys. Res.*, 104, 817–844, doi:10.1029/1998JB900007.
- Okubo, P. G. (1989), Dynamic rupture modeling with laboratory-derived constitutive relations, *J. Geophys. Res.*, 94, 12,321–12,335, doi:10.1029/JB094iB09p12321.
- Perfettini, H., and J.-P. Ampuero (2008), Dynamics of a velocity strengthening fault region: Implications for slow earthquakes and postseismic slip, *J. Geophys. Res.*, 113, B09411, doi:10.1029/2007JB005398.
- Rice, J. R., and Y. Ben-Zion (1996), Slip complexity in earthquake fault models, *Proc. Natl. Acad. Sci. U. S. A.*, 93, 3811–3818, doi:10.1073/pnas.93.9.3811.
- Rice, J. R., and A. L. Ruina (1983), Stability of steady frictional slipping, *J. Appl. Mech.*, 50, 343–349, doi:10.1115/1.3167042.
- Rubin, A. M., and J.-P. Ampuero (2005), Earthquake nucleation on (aging) rate and state faults, *J. Geophys. Res.*, 110, B11312, doi:10.1029/2005JB003686.
- Rubinstein, S. M., G. Cohen, and J. Fineberg (2004), Detachment fronts and the onset of dynamic friction, *Nature*, 430, 1005–1009, doi:10.1038/nature02830.
- Ruina, A. L. (1983), Slip instability and state variable friction laws, *J. Geophys. Res.*, 88, 10,359–10,370, doi:10.1029/JB088iB12p10359.

J.-P. Ampuero, Division of Geological and Planetary Sciences, California Institute of Technology, 1200 E. California Blvd., MC 252-21, Pasadena, CA 91125, USA. (ampuero@gps.caltech.edu)

Y. Kaneko, Institute of Geophysics and Planetary Physics, Scripps Institution of Oceanography, University of California, 9500 Gilman Dr., MC 0225, San Diego, La Jolla, CA 92093, USA. (ykaneko@ucsd.edu)